Nonlinear Dyn (2019) 98:1355–1363
https://doi.org/10.1007/s11071-019-05267-0

ORIGINAL PAPER

Design of adaptive sliding mode controllers for a class of perturbed fractional-order nonlinear systems

Chih-Chiang Cheng · **Shao-Chiang Hsu**

Received: 15 May 2019 / Accepted: 17 September 2019 / Published online: 23 September 2019

Abstract In this paper, a design methodology of the adaptive sliding mode controller was proposed for a class of multi-input fractional-order nonlinear systems with matched and unmatched perturbations to solve state regulation problems. The sliding surface is firstly introduced, and then the controller is designed with adaptive mechanisms and perturbation estimator embedded. Due to the employed adaptive and perturbation estimation mechanisms, the upper bounds of the perturbations and perturbation estimation errors do not need to be known in advance. The resultant control scheme is capable of driving the controlled states into the equilibrium point and stays thereafter within a finite time. Finally, a numerical example is given for demonstrating the feasibility of the proposed control scheme.

Keywords Sliding mode control · Fractional-order nonlinear systems · Unmatched perturbations

1 Introduction

Owing to fractional derivatives and integrals providing a powerful tool in describing the memory and hereditary properties of different substances, many researchers have recently pointed out that fractional calculus is well suited for modeling and describing of properties of many practical processes, such as thermal systems [1], power systems [2], financial systems [3], electromechanical systems [4], biological systems [5], hyperchaotic systems [6] and viscoelastic materials [7]. As a result, fractional calculus has also been applied to many practical applications by engineers and physicists [7–11].

Sliding mode control (SMC) is a well-known nonlinear control design method because of its robustness against matched perturbations encountered in the systems [12,13]. In the past few decades, SMC has been used in many different integer order (IO) systems such as mobile robots [14,15], DC–DC boost converters [16] and vehicle systems [17]. With the development of fractional calculus, the controls of FO systems by using SMC technique have also applied to various kinds of nonlinear systems [18–36]. However, it is noted that the designers have to know in advance the upper bounds of the perturbations when utilizing the control schemes proposed in [22–30], and in [19–36] designers only considered matched perturbations.

In order to alleviate or eliminate the restrictions of the researches mentioned above [18–36], in this paper, we also designed an adaptive sliding mode controller for a class of multi-input FO nonlinear systems with matched and unmatched perturbations to solve the regulation problems. The novelties of this research are as follows. (1) A fractional derivative estimator is proposed in this research, which can be utilized to estimate the perturbations encountered in the system, and

C.-C. Cheng (✉) · S.-C. Hsu
Department of Electrical Engineering, National Sun Yat-Sen University, No. 70, Lien Hai Rd., Kaohsiung, Taiwan, ROC
e-mail: chengcc@mail.ee.nsysu.edu.tw

adaptation mechanisms are embedded in the proposed control scheme so that the designers do not need to know in advance the upper bounds of the perturbations as well as perturbation estimation errors. (2) The dynamic equations of the plant considered in this research are more generalized than those in [27–33] since the control schemes in [27–33] do not allow the input gain uncertainty to appear in the second differential equation, and we replaced the state $\mathbf{x}_2$ in the first differential equation with function $\mathbf{g}(\mathbf{x}_2)$. The major improvement in the proposed control scheme is that it can be applied to a class of FO nonlinear systems with unmatched perturbations and it is capable of driving the state trajectory into the equilibrium point and stays thereafter within a finite time as well, which may not be achievable by using the control schemes developed in [19–36]. Finally, a numerical example is illustrated by using computer simulation for showing the feasibility of the proposed control scheme.

2 System descriptions and problem formulations

Consider a class of multi-input nonlinear FO systems with matched and unmatched perturbations governed by

$$\begin{aligned} D^{\alpha}\mathbf{x}_1 &= \mathbf{f}_1(t,\mathbf{x}_1) + \mathbf{G}_1(t,\mathbf{x}_1)\mathbf{g}(\mathbf{x}_2) + \triangle\mathbf{p}_1(t,\mathbf{x}), \\ D^{\alpha}\mathbf{x}_2 &= \mathbf{f}_2(t,\mathbf{x}) + \mathbf{G}_2(t,\mathbf{x})\mathbf{u} + \triangle\mathbf{p}_2(t,\mathbf{x},\mathbf{u}), \end{aligned} \tag{1}$$

where $\alpha \in R$ and $\alpha \in (0,1)$; $\mathbf{x} \triangleq [\mathbf{x}_1^T \ \ \mathbf{x}_2^T]^T \in R^n$ is the measurable state vector, $\mathbf{x}_2 \in R^{m\times 1}$, $\mathbf{g}(\mathbf{x}_2) \in R^{m\times 1}$, $\mathbf{x}_1 \triangleq [x_{11}, x_{12}, \ldots, x_{1(n-m)}]^T \in R^{n-m}$, and $n \le 2m$. The nonlinear vectors $\mathbf{f}_1(t,\mathbf{x}_1)$, $\mathbf{f}_2(t,\mathbf{x})$ and $\mathbf{g}(\mathbf{x}_2)$ are known, and $\mathbf{f}_1(t,\mathbf{x}_1) = \mathbf{0}$ if $\mathbf{x}_1 = \mathbf{0}$. The matrices $\mathbf{G}_1$ and $\mathbf{G}_2$ are also known. The vector $\mathbf{u} \in R^{s\times 1}$ is the control input, and $m \le s$. The vectors $\triangle\mathbf{p}_i(\bullet)$, $1 \le i \le 2$, are unknown uncertainties, parameter variations and/or external disturbances. The aim of this paper is to design a sliding mode controller with perturbation estimation scheme such that the state trajectory $\mathbf{x}(t)$ of (1) can reach zero within a finite time. In order to achieve this purpose, we assume that the following assumptions are valid throughout this paper:
A1: The matrices $\mathbf{G}_1(t,\mathbf{x}_1)$ and $\mathbf{G}_2(t,\mathbf{x})$ have full row rank for all $\mathbf{x}$ and t in the domain of interest; these imply that the matrices $\mathbf{G}_j^+ \triangleq \mathbf{G}_j^T(\mathbf{G}_j\mathbf{G}_j{}^T)^{-1}$, $j = 1, 2$, exist.

A2: The vector $\mathbf{f}_1(t,\mathbf{x}_1)$ and matrix $\mathbf{G}_1^+$ are continuously differentiable with respect to $\mathbf{x}_1$.
A3: [37] The unmatched and matched perturbations fulfill the following inequalities

$$\|\triangle\mathbf{p}_1(t,\mathbf{x})\| \le \gamma_1\beta_1(\mathbf{x}), \ \ \|\triangle\mathbf{p}_2(t,\mathbf{x},\mathbf{u})\| \le \beta_2(\mathbf{x},\mathbf{u}),$$

in the domain of interest for all t and $\mathbf{x}$, where γ_1 is an unknown positive constant, $\beta_1(\mathbf{x})$ is a known positive function, and $\beta_2(\mathbf{x},\mathbf{u})$ is an unknown positive function. In addition, $\beta_1(\mathbf{x}) = 0$ if $\mathbf{x} = \mathbf{0}$, and the function $\beta_2(\mathbf{x},\mathbf{u})$ is bounded if $\mathbf{x}$ and $\mathbf{u}$ are bounded. In this paper, the notation $\|\cdot\|$ stands for the Euclidean norm of a vector or the induced two-norm of a matrix.
A4: $\mathbf{g}(\mathbf{x}_2) = \mathbf{0}$ implies $\mathbf{x}_2 = \mathbf{0}$, and $\left(\partial\mathbf{g}/\partial\mathbf{x}_2\right)^{-1}$ exists.

Remark 1 The vector $\mathbf{g}(\mathbf{x}_2)$ of plant (1) considered in [27–33] is $\mathbf{g}(\mathbf{x}_2) = \mathbf{x}_2$; however, the vector $\mathbf{g}(\mathbf{x}_2)$ considered in this paper may be a function of $\mathbf{x}_2$.

The following theorem will be utilized in the stability analysis in Sect. 6.

Theorem 1 *If there exists a continuous and positive definite function $V(\mathbf{x}(t),t)$ satisfying the following differential inequality:*

$$D^{\alpha}V(\mathbf{x}(t),t) \le -k, \tag{2}$$

where k is a positive constant, and $\alpha \in (0,1)$, then $V \equiv 0, \forall t \ge T$. The finite time T is given by

$$T = \left(\frac{\Gamma(\alpha+1)}{k}V(\mathbf{x}_0,0)\right)^{\frac{1}{\alpha}}, \tag{3}$$

where $t_0 = 0$ is initial time and $\Gamma(x) \triangleq \int_0^{\infty} e^{-t}t^{x-1}dt$ is the Euler's Gamma function [38].

Proof From (2), it is seen that

$$D^{\alpha}\left(\int_0^t \dot{V}(\mathbf{x}(\tau),\tau)\mathrm{d}\tau\right) \le -k. \tag{4}$$

Multiplying fractional integral operator $D^{-\alpha}$ to both side of (4), we obtain

$$\int_0^t \dot{V}(\mathbf{x}(\tau),\tau)d\tau \le D^{-\alpha}(-k). \tag{5}$$

By using the following equation [38],

$${}_{t_0}D_t^{-\alpha}f(t) = \frac{1}{\Gamma(\alpha)}\int_{t_0}^t \frac{f(\tau)}{(t-\tau)^{1-\alpha}}\mathrm{d}\tau,$$

From (5), we obtain

$$\int_0^t \dot{V}(\mathbf{x}(\tau),\tau)\mathrm{d}\tau \le -k\frac{1}{\Gamma(\alpha)}\int_0^t \frac{1}{(t-\tau)^{1-\alpha}}\mathrm{d}\tau = -\frac{kt^{\alpha}}{\alpha\Gamma(\alpha)}. \tag{6}$$

Then by using the reduction formula $\Gamma(x+1) = x\Gamma(x)$ [39], from (6) one can obtain

$$V(\mathbf{x}(t),t) - V(\mathbf{x}_0,0) \le -\frac{kt^{\alpha}}{\Gamma(\alpha+1)}.$$

The preceding equation also implies that the finite time T is given by (3). □

3 Design of sliding surface

According to the methodology of sliding mode control, one should design a sliding surface function $\boldsymbol{\sigma}$ and a control function $\mathbf{u}$ such that once the controlled system enters the sliding surface and remains on the surface thereafter, the desired system's performance and control's objective can be realized. Hence in the first step, we design the sliding surface function as

$$\boldsymbol{\sigma}(\mathbf{x}_1) = \mathbf{x}_1. \tag{7}$$

By using (1), one obtains the fractional derivative of $\boldsymbol{\sigma}$ from (7) as

$$D^{\alpha}\boldsymbol{\sigma} = D^{\alpha}\mathbf{x}_1 = \mathbf{f}_1 + \mathbf{G}_1\mathbf{g}(\mathbf{x}_2) + \triangle\mathbf{p}_1. \tag{8}$$

Design another function $\boldsymbol{\phi}$ as

$$\boldsymbol{\phi}(t,\mathbf{x}) = \mathbf{g}(\mathbf{x}_2) - \boldsymbol{\eta}(t,\mathbf{x}_1), \tag{9}$$

where

$$\boldsymbol{\eta}(t,\mathbf{x}_1) = \begin{cases} -\mathbf{G}_1^{+}\left[\mathbf{f}_1(t,\mathbf{x}_1) + \hat{\gamma}_1(t)\|\boldsymbol{\zeta}_1(\boldsymbol{\sigma})\|\boldsymbol{\sigma} + \lambda_1\frac{\boldsymbol{\sigma}}{\|\boldsymbol{\sigma}\|}\right], \\ \text{if} \quad \boldsymbol{\sigma} \neq \mathbf{0} \\ \mathbf{0}, \quad \text{if} \quad \boldsymbol{\sigma} = \mathbf{0} \end{cases} \tag{10}$$

The scalar λ_1 is a designed positive constant, and the adaptive gain $\hat{\gamma}_1(t) \ge 0,\ \forall t$ will be introduced later. For obtaining the function $\boldsymbol{\zeta}_1$ in (10), one can utilize the similar method as in [37] to compute the upper bound of $\triangle\mathbf{p}_1$ as

$$\|\triangle\mathbf{p}_1(t,\mathbf{x})\| \le \gamma_1\|\boldsymbol{\zeta}_1(\boldsymbol{\sigma})\|\|\boldsymbol{\sigma}\| + \gamma_1\|\boldsymbol{\zeta}_2(\boldsymbol{\sigma},\boldsymbol{\phi})\|\|\boldsymbol{\phi}\|, \tag{11}$$

where

$$\boldsymbol{\zeta}_1(\boldsymbol{\sigma}) = \int_0^1 \frac{\partial\beta_1(\boldsymbol{\mu}_1,\mathbf{0})}{\partial\boldsymbol{\mu}_1}\Big|_{\boldsymbol{\mu}_1=\boldsymbol{\sigma}\omega}\mathrm{d}\omega \in R^{(n-m)\times 1},$$

$$\boldsymbol{\zeta}_2(\boldsymbol{\sigma},\boldsymbol{\phi}) = \int_0^1 \frac{\partial\beta_1(\boldsymbol{\sigma},\boldsymbol{\mu}_2)}{\partial\boldsymbol{\mu}_2}\Big|_{\boldsymbol{\mu}_2=\boldsymbol{\phi}\omega}\mathrm{d}\omega \in R^{m\times 1}.$$

Substituting (9) and (10) into (8), one can see that the dynamic equation of $\boldsymbol{\sigma}$ for $\boldsymbol{\sigma} \neq \mathbf{0}$ is

$$D^{\alpha}\boldsymbol{\sigma} = -\lambda_1\frac{\boldsymbol{\sigma}}{\|\boldsymbol{\sigma}\|} - \hat{\gamma}_1(t)\|\boldsymbol{\zeta}_1(\boldsymbol{\sigma})\|\boldsymbol{\sigma} + \triangle\mathbf{p}_1 + \mathbf{G}_1\boldsymbol{\phi}. \tag{12}$$

Now define the first Lyapunov function candidate as

$$V_1 = \|\boldsymbol{\sigma}\| + \frac{1}{2}\tilde{\gamma}_1^2, \tag{13}$$

where $\tilde{\gamma}_1(t) \triangleq \hat{\gamma}_1(t) - \gamma_1$ is the adaptive error of the unknown constant γ_1. By using (11), we can obtain the fractional derivative of (13) along the trajectory of (12) for $\boldsymbol{\sigma} \neq \mathbf{0}$ as

$$\begin{aligned} D^{\alpha}V_1 &\le \frac{\boldsymbol{\sigma}^T}{\|\boldsymbol{\sigma}\|}\Big\{-\lambda_1\frac{\boldsymbol{\sigma}}{\|\boldsymbol{\sigma}\|} - \hat{\gamma}_1(t)\|\boldsymbol{\zeta}_1(\boldsymbol{\sigma})\|\boldsymbol{\sigma} + \triangle\mathbf{p}_1 + \mathbf{G}_1\boldsymbol{\phi}\Big\} + \tilde{\gamma}_1 D^{\alpha}\hat{\gamma}_1 \\ &\le -\lambda_1 - \big(\hat{\gamma}_1(t) - \gamma_1\big)\|\boldsymbol{\zeta}_1(\boldsymbol{\sigma})\|\|\boldsymbol{\sigma}\| + \gamma_1\|\boldsymbol{\zeta}_2(\boldsymbol{\sigma},\boldsymbol{\phi})\| \\ &\quad \times \|\boldsymbol{\phi}\| + \frac{\boldsymbol{\sigma}^T}{\|\boldsymbol{\sigma}\|}\mathbf{G}_1\boldsymbol{\phi} + \big(\hat{\gamma}_1(t) - \gamma_1\big)D^{\alpha}\hat{\gamma}_1. \end{aligned} \tag{14}$$

According to (14), one may design the adaptive gain $\hat{\gamma}_1(t)$ for adapting the unknown constant γ_1 as

$$D^{\alpha}\hat{\gamma}_1(t) = \|\boldsymbol{\zeta}_1(\boldsymbol{\sigma})\|\|\boldsymbol{\sigma}\|, \quad \hat{\gamma}_1(0) = 0. \tag{15}$$

Substituting (15) into (14) for $\boldsymbol{\sigma} \neq \mathbf{0}$ yields

$$D^{\alpha}V_1 \le -\lambda_1 + \gamma_1\|\boldsymbol{\zeta}_2(\boldsymbol{\sigma},\boldsymbol{\phi})\|\|\boldsymbol{\phi}\| + \frac{\boldsymbol{\sigma}^T}{\|\boldsymbol{\sigma}\|}\mathbf{G}_1\boldsymbol{\phi}. \tag{16}$$

If $\boldsymbol{\sigma} = \mathbf{0}$, then from (13) and (15), one can obtain $V_1 = \tilde{\gamma}_1^2/2$ and $D^{\alpha}\hat{\gamma}_1 = 0$. Hence $D^{\alpha}V_1 \le \tilde{\gamma}_1 D^{\alpha}\tilde{\gamma} = \tilde{\gamma}_1 D^{\alpha}\hat{\gamma}_1 = 0$. Therefore, it can be seen that, if state $\boldsymbol{\phi}$ reaches zero in a finite time and stays thereafter, i.e., $\boldsymbol{\phi} = \mathbf{0}$ and $D^{\alpha}\boldsymbol{\phi} = \mathbf{0}$ (this will be shown in Sect. 6), Eq. (16) becomes $D^{\alpha}V_1 \le -\lambda_1$. Hence the Lyapunov function V_1 will converge to zero within a finite time if $\boldsymbol{\sigma} \neq \mathbf{0}$ in accordance with Theorem 1, and V_1 will stop

decreasing if $\boldsymbol{\sigma} = \mathbf{0}$. Therefore, the sliding variable $\boldsymbol{\sigma}$ will also reach zero within a finite time. Note that $\hat{\gamma}_1(t)$ will reach a finite nonzero limit in accordance with (15), and this will be explained in Sect. 6.

On the other hand, when the controlled system enters the sliding surface in a finite time, from (7) and (10) one can see that the state $\mathbf{x}_1 = \mathbf{0}$ and $\boldsymbol{\eta}(t, \mathbf{x}_1) = \mathbf{0}$ within a finite time too. According to (9), vector $\mathbf{g}(\mathbf{x}_2)$ will tend to zero within a finite time. Hence the state $\mathbf{x}_2$ will also tend to zero in accordance with assumption **A4**.

4 Design of fractional derivative estimator

In order to reduce the chattering phenomenon and save control energy, we propose a design method of fractional derivative estimator (FDE). The idea of designing this FDE is quite similar to that of AIVSDE developed by Cheng and Chang [40]. The block diagram of the proposed FDE is shown in Fig. 1, where $r(t)$ is the input signal, $\hat{k}_r(t)$ is an adaptive gain, which will be explained later. The notation $D^{-\alpha}$ stands for the fractional integral operator; k_1, k_2, and k_b are adjustable positive constant gains specified by the designer and $y(t)$ is output.

The idea of designing the FDE shown in Fig. 1 is to force the magnitude of the error signal $e(t)$ to be as small as possible in a finite time. Then the signal $x(t)$ will approach the signal $r(t)$, and the output signal $y(t)$ in Fig. 1 will approach the fractional derivative of the input signal $r(t)$ since $y(t) = D^{\alpha}x(t)$.

The following theorem proves that under certain mild conditions the signal $\sigma(t)$ depicted in Fig. 1 will approach zero in a finite time, and the fractional derivative estimation error $e(t)$ will be asymptotically stable.

Theorem 2 *Consider the FDE shown in Fig. 1 with* $k_2 > 1$. *Suppose that* $|r(t)| \le \bar{k}_0$ *and* $|D^{\alpha}r(t)| \le \bar{k}_1$ *are fulfilled in a finite time, where* $\bar{k}_0$ *and* $\bar{k}_1$ *are unknown constants. The adaptive gain* $\hat{k}_r(t)$ *is given by the adaptive law*

$$D^{\alpha}\hat{k}_r(t) = \begin{cases} \beta_r, & \text{if } \sigma(t) \neq 0 \\ 0, & \text{if } \sigma(t) = 0 \end{cases}, \quad \hat{k}_r(0) = \delta > 0$$

where β_r *is a designed positive constant. Then* $\sigma(t)$ *will approach zero within a finite time, the fractional derivative estimation error* $e(t)$ *will reach zero asymptotically, and the adaptive gain* $\hat{k}_r(t)$ *is bounded.*

Proof The proof of this theorem is very similar to that in [40], and hence it is omitted in this paper. □

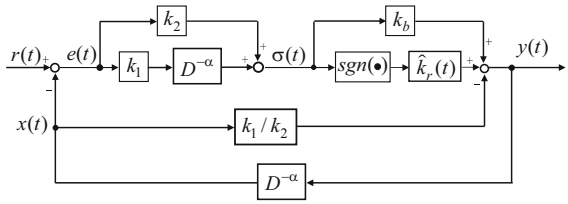

Fig. 1 Block diagram of fractional derivative estimator

5 Design of controllers

In order to drive the state trajectories of the controlled system into the designated sliding surface in a finite time, we design the proposed controller as

$$\mathbf{u} = -\mathbf{G}_2^{+}[\mathbf{u}_f + \mathbf{u}_s], \tag{17}$$

where

$$\mathbf{u}_f = \mathbf{f}_2 + \boldsymbol{\psi}(t) + \left(\frac{\partial \mathbf{g}}{\partial \mathbf{x}_2}\right)^{-1}\left(c_0\boldsymbol{\phi} + \mathbf{p}_{\text{est}}(t)\right), \tag{18}$$

$$\mathbf{u}_s = \begin{cases} \left(\frac{\partial \mathbf{g}}{\partial \mathbf{x}_2}\right)^{-1}\left(\left[-c_0\|\boldsymbol{\phi}\| + \lambda_2 + \hat{\gamma}_2(t)\beta_3(\mathbf{x})\right]\frac{\boldsymbol{\phi}(t)}{\|\boldsymbol{\phi}(t)\|}\right), \\ \text{if } \boldsymbol{\phi} \neq \mathbf{0} \\ \mathbf{0}, \quad \text{if } \boldsymbol{\phi} = \mathbf{0} \end{cases} \tag{19}$$

where c_0 and λ_2 are designed positive constants. In addition, the adaptive laws $\hat{\gamma}_2(t)$ and $\boldsymbol{\psi}(t)$ are specified, respectively, as

$$D^{\alpha}\hat{\gamma}_2(t) = \begin{cases} \beta_3(\mathbf{x}), & \text{if } \boldsymbol{\phi} \neq \mathbf{0} \\ \mathbf{0}, & \text{if } \boldsymbol{\phi} = \mathbf{0} \end{cases}, \quad \hat{\gamma}_2(0) = 0 \tag{20}$$

$$D^{\alpha}\boldsymbol{\psi}(t) = \begin{cases} -\left[h_1\delta(\mathbf{u}) + h_2\|\boldsymbol{\psi}\|\right]\frac{\boldsymbol{\psi}(t)}{\|\boldsymbol{\psi}(t)\|}, & \text{if } \boldsymbol{\psi}(t) \neq \mathbf{0} \\ -\boldsymbol{\theta}, & \text{if } \boldsymbol{\psi}(t) = \mathbf{0} \end{cases} \tag{21}$$

where $\boldsymbol{\theta}$ is a designed vector with positive entries. The other positive constants h_1, h_2 and functions $\delta(\mathbf{u})$, $\beta_3(\mathbf{x})$ are introduced in the next section.

The perturbation estimation signal $\mathbf{p}_{\text{est}}(t)$ in (18) is designed in a similar way as in [37]. By using (1), (9) and (17), one can see that

$$D^{\alpha}\boldsymbol{\phi} = \frac{\partial \mathbf{g}}{\partial \mathbf{x_2}}(-\boldsymbol{\psi}(t) - \mathbf{u}_s + \triangle \mathbf{p}_2) - c_0\boldsymbol{\phi} - \mathbf{p}_{\text{est}} - D^{\alpha}\boldsymbol{\eta}. \tag{22}$$

Now design a nominal signal $\boldsymbol{\phi}_{(\text{nom})}(t)$ as

$$D^{\alpha}\boldsymbol{\phi}_{(\text{nom})} = -c_0\boldsymbol{\phi}_{(\text{nom})} - \mathbf{p}_{\text{est}} - \frac{\partial \mathbf{g}}{\partial \mathbf{x_2}}\mathbf{u}_s, \tag{23}$$

where $c_0 > \alpha\pi/2$. Then subtracting (23) from (22) yields

$$D^{\alpha}\big(\boldsymbol{\phi} - \boldsymbol{\phi}_{(\text{nom})}\big) + c_0\big(\boldsymbol{\phi} - \boldsymbol{\phi}_{(\text{nom})}\big) = \frac{\partial \mathbf{g}}{\partial \mathbf{x_2}}\Big(-\boldsymbol{\psi}(t) + \triangle \mathbf{p}_2\Big) - D^{\alpha}\boldsymbol{\eta}. \tag{24}$$

Let $\hat{\mathbf{p}}(t)$ be the output of the FDE developed in Sect. 4. This FDE is used to estimate the signal $D^{\alpha}\big(\boldsymbol{\phi} - \boldsymbol{\phi}_{(\text{nom})}\big)$ since $\boldsymbol{\phi}$ and $\boldsymbol{\phi}_{(\text{nom})}$ are measurable and differentiable. Hence one obtains that

$$\hat{\mathbf{p}}(t) = D^{\alpha}\big(\boldsymbol{\phi} - \boldsymbol{\phi}_{(\text{nom})}\big) + \boldsymbol{\omega}(t), \tag{25}$$

where $\boldsymbol{\omega}(t)$ is the fractional derivative estimation error. If the FDE is designed properly, then $\boldsymbol{\omega}(t)$ is small in accordance with Theorem 2.

The perturbation estimation signal in this paper is then designed as

$$\mathbf{p}_{\text{est}} = \hat{\mathbf{p}}(t) + c_0\big(\boldsymbol{\phi} - \boldsymbol{\phi}_{(\text{nom})}\big). \tag{26}$$

The block diagram for implementing the signal $\mathbf{p}_{\text{est}}$ is depicted in Fig. 2. From (24), (25), and (26), one can define the perturbation estimation error as

$$\triangle\tilde{\mathbf{p}}_2(t) \triangleq \frac{\partial \mathbf{g}}{\partial \mathbf{x_2}}\big[-\boldsymbol{\psi}(t) + \triangle \mathbf{p}_2\big] - D^{\alpha}\boldsymbol{\eta} - \mathbf{p}_{\text{est}} = -\boldsymbol{\omega}(t). \tag{27}$$

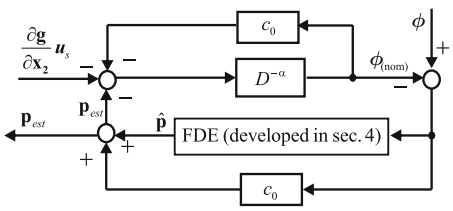

Fig. 2 Perturbation estimation mechanism for computing $\mathbf{p}_{\text{est}}$

6 Stability analysis

According to the analysis in Sect. 3, one can see that the trajectory of $\mathbf{x}$ will reach zero within a finite time once the state $\boldsymbol{\phi}$ approaches zero and stays thereafter. Therefore, the main purpose of this section is to show that the designed controller (17) indeed has the ability to drive the trajectory of $\boldsymbol{\phi}$ to zero in a finite time. The stability of the proposed control system is addressed in the following theorem.

Theorem 3 *Consider the dynamic system* (1) *with assumptions* **A1** *to* **A4**. *Suppose that there exist known positive constants* h_1, h_2, *and an unknown positive constant* γ_2 *satisfying the following inequality*

$$\|\triangle\tilde{\mathbf{p}}_2(t)\| \le \gamma_2\beta_3(\mathbf{x}) + h_1\delta(\mathbf{u}) + h_2\|\boldsymbol{\psi}(t)\| \tag{28}$$

$\forall\, t$, $\mathbf{x}$ *in the domain of interest, where* $\beta_3(\mathbf{x})$ *and* $\delta(\mathbf{u})$ *are known positive functions and* $\boldsymbol{\psi}(t)$ *is the state variable defined in* (21).

If the controller (17) *with adaptive laws* (15), (20) *and* (21) *are employed, then*

(a) *the function* $\boldsymbol{\phi}$ *and state variable* $\mathbf{x}$ *will approach zero within a finite time;*

(b) *the adaptive gains* $\hat{\gamma}_1$ *and* $\hat{\gamma}_2$ *are all bounded, and* $\hat{\gamma}_1, \hat{\gamma}_2$ *will reach a finite limit, respectively, as* $t \to \infty$*;*

(c) *the nominal signal* $\boldsymbol{\phi}_{(\text{nom})}$ *and the estimation signal* $\mathbf{p}_{\text{est}}(t)$ *are all bounded.*

Proof (a) Define the second Lyapunov function candidate as

$$V_2 = \|\boldsymbol{\phi}\| + \frac{1}{2}\tilde{\gamma}_2^2 + \|\boldsymbol{\psi}\|, \tag{29}$$

where $\tilde{\gamma}_2(t) \triangleq \hat{\gamma}_2(t) - \gamma_2$ is the adaptive error of the unknown positive constant γ_2. All the possible cases that may occur in the derivative of (29) are analyzed as follows.

Case 1 : $\boldsymbol{\phi} \neq \mathbf{0}$ and $\boldsymbol{\psi} \neq \mathbf{0}$

By using (19), (27) and (28), one computes the fractional derivative of (29) along the trajectories of (22) and (20) as

$$\begin{aligned} D^{\alpha}V_2 &\le \frac{\boldsymbol{\phi}^T}{\|\boldsymbol{\phi}\|}D^{\alpha}\boldsymbol{\phi} + \tilde{\gamma}_2 D^{\alpha}\hat{\gamma}_2 + \frac{\boldsymbol{\psi}^T(t)}{\|\boldsymbol{\psi}(t)\|}D^{\alpha}\boldsymbol{\psi} \\ &= -\lambda_2 - \hat{\gamma}_2\beta_3(\mathbf{x}) + \frac{\boldsymbol{\phi}^T}{\|\boldsymbol{\phi}\|}\triangle\tilde{\mathbf{p}}_2(t) + \tilde{\gamma}_2 D^{\alpha}\hat{\gamma}_2 \\ &\quad + \frac{\boldsymbol{\psi}^T(t)}{\|\boldsymbol{\psi}(t)\|}D^{\alpha}\boldsymbol{\psi} \end{aligned}$$

$$\leq -\lambda_2 - \hat{\gamma}_2\beta_3(\mathbf{x}) + \gamma_2\beta_3(\mathbf{x}) + h_1\delta(\mathbf{u}) + h_2\|\boldsymbol{\psi}\| + (\hat{\gamma}_2 - \gamma_2)D^\alpha\hat{\gamma}_2 + \frac{\boldsymbol{\psi}^T(t)}{\|\boldsymbol{\psi}(t)\|}D^\alpha\boldsymbol{\psi}$$
$$= -\lambda_2 + h_1\delta(\mathbf{u}) + h_2\|\boldsymbol{\psi}\| + \frac{\boldsymbol{\psi}^T(t)}{\|\boldsymbol{\psi}(t)\|}D^\alpha\boldsymbol{\psi}. \quad (30)$$

By using (21), one can further simplify (30) as

$$D^\alpha V_2 \leq -\lambda_2 < 0. \quad (31)$$

Equation (31) clearly indicates that the function V_2 is bounded, hence the trajectories of $\boldsymbol{\phi}$, $\hat{\gamma}_2$ and $\boldsymbol{\psi}$ are all bounded, and the state $\boldsymbol{\phi}$ will be driven toward zero within a finite time in this case. Noted that the state $\boldsymbol{\psi}$ is asymptotically stable due to $\boldsymbol{\psi}^T D^\alpha\boldsymbol{\psi} < 0$ in accordance with (21), and it also means that the state $\boldsymbol{\psi}$ will not reach zero and stay thereafter in a finite time. The adaptive gain $\hat{\gamma}_2$ will not reach zero in a finite time either, this is explained in part (b). When $\boldsymbol{\phi}$ reaches zero in a finite time, the stability of the controlled system is analyzed in case 3 and case 4.

Case 2 : $\boldsymbol{\phi} \neq \mathbf{0}$ and $\boldsymbol{\psi} = \mathbf{0}$
From the fractional derivative of (30), it is seen that

$$D^\alpha V_2 \leq -\lambda_2 + h_1\delta(\mathbf{u}).$$

In this case, $D^\alpha V_2$ may be greater or smaller than zero. From (21), it is seen that $\boldsymbol{\psi} = \mathbf{0}$ and $D^\alpha\boldsymbol{\psi} \neq \mathbf{0}$, it means that the trajectory of $\boldsymbol{\psi}$ will not stay in the surface $\boldsymbol{\psi} = \mathbf{0}$ and will cross the surface $\boldsymbol{\psi} = \mathbf{0}$ immediately (that is, $\boldsymbol{\psi} \neq \mathbf{0}$ in the next time interval). Hence the status of the system will switch to another case with $\boldsymbol{\psi} \neq \mathbf{0}$. Noted that the states $\boldsymbol{\phi}$ and $\hat{\gamma}_2$ are still bounded in this case due to the continuity of these trajectories.

Case 3 : $\boldsymbol{\phi} = \mathbf{0}$ and $\boldsymbol{\psi} \neq \mathbf{0}$
From (29), it is seen $V_2 = \frac{1}{2}\tilde{\gamma}_2^2 + \|\boldsymbol{\psi}\|$. By noting that $D^\alpha\hat{\gamma}_2 = 0$ in (20), and using (21) for $\boldsymbol{\psi} \neq \mathbf{0}$, one is able to compute $D^\alpha V_2$ as

$$D^\alpha V_2 = \frac{\boldsymbol{\psi}^T(t)}{\|\boldsymbol{\psi}(t)\|}D^\alpha\boldsymbol{\psi} = -h_1\delta(\mathbf{u}) - h_2\|\boldsymbol{\psi}\| < 0.$$

One can see that V_2 is a bounded function and the magnitude of V_2 will still decrease in this case. Hence one can conclude that $\boldsymbol{\psi}$ and $\hat{\gamma}_2(t)$ are bounded in this case.

Case 4 : $\boldsymbol{\phi} = \mathbf{0}$ and $\boldsymbol{\psi} = \mathbf{0}$
In this case, it is seen that $V_2 = \frac{1}{2}\tilde{\gamma}_2^2$. Hence $D^\alpha V_2 = 0$ in accordance with (20). Therefore, the value of V_2 will not decrease and both V_2 and $\hat{\gamma}_2(t)$ are bounded in this case.

According to the previous stability analysis from case 1 to case 4 and Theorem 1, it can be seen that variable $\boldsymbol{\phi}(t)$ will approach zero and stay thereafter in a finite time. According to (16), the Lyapunov function V_1 will also converge to zero in a finite time once $\boldsymbol{\phi} = \mathbf{0}$. Therefore, the controlled state variable $\mathbf{x}$ will tend to zero within a finite time in accordance with the analysis of Sect. 3.

(b) From (15) and (20), it is seen that adaptive gains $\hat{\gamma}_j(t)$, $j = 1, 2$, are monotonically increasing and are all bounded above in accordance with the analysis of part (a). Therefore, there exist finite constants $\gamma_{j\infty}$, $j = 1, 2$, such that $\lim_{t\to\infty}\hat{\gamma}_j(t) = \gamma_{j\infty}$, $j = 1, 2$ [41] (Proposition 2.14, page 83).

(c) According to (10), one can see that the function $\boldsymbol{\eta}$ depends on state $\mathbf{x}_1$ and t, and hence the fractional derivative of $\boldsymbol{\eta}$ is given by

$$D^\alpha\boldsymbol{\eta} = \frac{\partial\boldsymbol{\eta}}{\partial\mathbf{x}_1}D^\alpha\mathbf{x}_1 + \frac{\partial\boldsymbol{\eta}}{\partial t} = \frac{\partial\boldsymbol{\eta}}{\partial\mathbf{x}_1}\left[\mathbf{f}_1 + \mathbf{G}_1\mathbf{g}(\mathbf{x}_2) + \Delta\mathbf{p}_1(t,\mathbf{x})\right] + \frac{\partial\boldsymbol{\eta}}{\partial t}. \quad (32)$$

According to the previous stability analysis, the states $\mathbf{x}_1, \mathbf{x}_2$ and $\boldsymbol{\eta}$ are all bounded and will approach zero within a finite time, which also implies that $D^\alpha\boldsymbol{\eta}$ is bounded in accordance with (32). Since $\boldsymbol{\psi}^T D^\alpha\boldsymbol{\psi} < 0$ in (21), the signal $\boldsymbol{\psi}$ is bounded. Hence the right-hand side of (24) is bounded in accordance with the assumption **A3** and the analysis of part (a). Hence according to Theorem 4.3 in [42], one can see that $\boldsymbol{\phi} - \boldsymbol{\phi}_{(\text{nom})}$ is bounded since $\frac{\partial\mathbf{g}}{\partial\mathbf{x}_2}\big(-\boldsymbol{\psi}(t) + \Delta\mathbf{p}_2\big) - D^\alpha\boldsymbol{\eta}$ is bounded and $c_0 > \alpha\pi/2$. Therefore, $\boldsymbol{\phi}_{(\text{nom})}$ must be bounded, and from (26) the signal $\mathbf{p}_{\text{est}}$ must be bounded due to $\hat{\mathbf{p}}(t)$ is bounded. □

Note that: The function $\beta_3(\mathbf{x})$ may be a non-vanishing function.

7 Numerical example

Consider a multi-input perturbed nonlinear FO system described by (1), where the fractional order is

$\alpha = 0.65$, and $\mathbf{g}(\mathbf{x}) = [x_{21} + x_{22} \quad x_{22} \quad x_{21} + x_{23}]^T$. The state variables are $\mathbf{x_1} \triangleq [x_{11} \quad x_{12}]^T$, $\mathbf{x_2} \triangleq [x_{21} \quad x_{22} \quad x_{23}]^T$. The known nonlinear vectors and matrices $\mathbf{f}_i$, $\mathbf{G}_i$, $1 \leq i \leq 2$, are given by $\mathbf{f}_1(t, \mathbf{x}_1) = [\sin(t)x_{11}^2 \quad x_{12}^2]^T$, $\mathbf{f}_2(t, \mathbf{x}) = [x_{11}x_{21}\cos(t) \cos(x_{12})x_{22} \quad x_{23}^2 x_{22} + \sin(t)]^T$,

$$\mathbf{G}_1(t, \mathbf{x}_1) = \begin{bmatrix} x_{12}\sin(t) & x_{11}^2 & 1 \\ 0 & 1 & \cos(x_{11}) \end{bmatrix},$$

$$\mathbf{G}_2(t, \mathbf{x}) = \begin{bmatrix} 5 & \cos(t) & x_{22}x_{12} \\ 1 & 2 & 0 \\ \sin(t) & \sin(x_{11}x_{22}) & 3 \end{bmatrix}.$$

The vector $\mathbf{u} \triangleq [u_1 \quad u_2 \quad u_3]^T$ represents the control input. For demonstrating the robustness of the proposed control scheme and computer simulation, we assume that the unknown perturbations $\triangle\mathbf{p}_i$, $1 \leq i \leq 2$, are

$$\triangle\mathbf{p}_1(t, \mathbf{x}) = \begin{bmatrix} 0.5x_{21}\cos(x_{11}t) \\ -x_{21}x_{22}^2 \end{bmatrix},$$

$$\triangle\mathbf{p}_2(t, \mathbf{x}, \mathbf{u}) = \begin{bmatrix} -x_{12}^2 u_2 \\ \sin(t)u_3 \\ x_{12}x_{23}^2 + \sin(t) \end{bmatrix}.$$

The controller and sliding surface function are designed in accordance with (17) and (7), respectively. The designed parameters are chosen to be $(\lambda_1, \lambda_2, c_0, h_1, h_2, k_1, k_2, k_b) = (0.1, 3, 25, 1, 1, 1, 5, 2)$, $\boldsymbol{\theta} = [0.1 \quad 0.1 \quad 0.1]^T$. The nonlinear positive vanishing functions β_1 in assumption **A3**, β_3 and $\delta(\mathbf{u})$ in (28) are given by

$$\delta(\mathbf{u}) \triangleq \|\mathbf{u}\|, \quad \beta_1(\mathbf{x}) \triangleq \|\mathbf{x}_1\|\|\mathbf{x}_2\| + \|\mathbf{x}_2\|^2,$$
$$\beta_3(\mathbf{x}) \triangleq 0.2\|\mathbf{x}_1\|\|\mathbf{x}_2\| + 0.25\|\mathbf{x}_1\|\|\mathbf{x}_2\|^2 + 0.3.$$

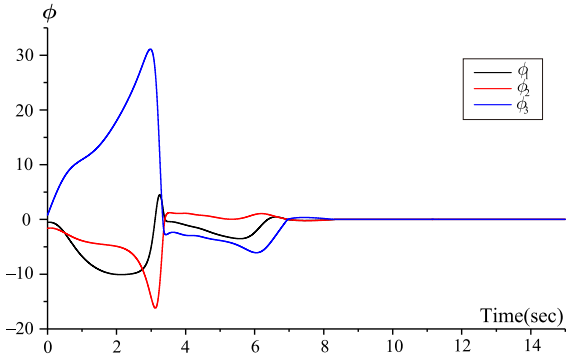

Fig. 3 The trajectory of function $\boldsymbol{\phi}$

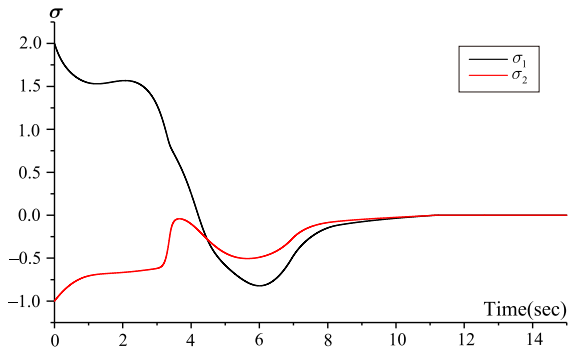

Fig. 4 The trajectory of sliding surface $\boldsymbol{\sigma}$

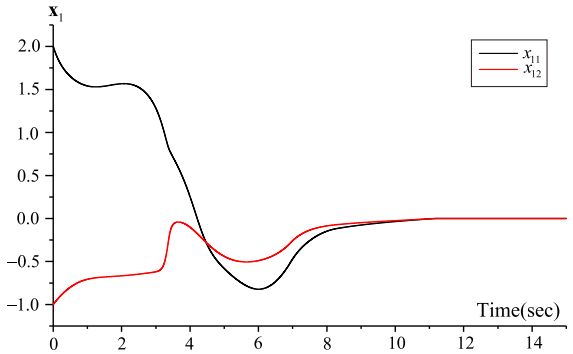

Fig. 5 The trajectory of state variable $\mathbf{x}_1$

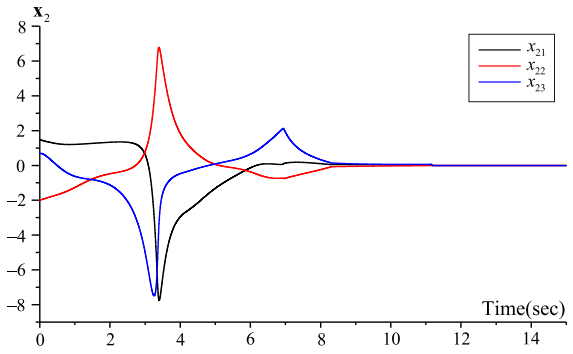

Fig. 6 The trajectory of state variable $\mathbf{x}_2$

The initial condition $\mathbf{x}(0)$ is assumed to be $\mathbf{x}(0) = [2 \quad -1 \quad 1.5 \quad -2 \quad 0.7]^T$. The results of computer simulation with step time 0.0001 s are shown from Figs. 3, 4, 5, 6, 7, 8 and 9. Figure 3 shows that the function $\boldsymbol{\phi}$ tends to zero within 8.32 s, and the controlled system enters the sliding surface in 11.19 s, as displayed in Fig. 4. The state variables $\mathbf{x}_i$, $1 \leq i \leq 2$, as illustrated in Figs. 5 and 6, all reach zero within 11.21 s. The functions $\boldsymbol{\phi}_{(\text{nom})}$, adaptive gains $\hat{\gamma}_1$, $\hat{\gamma}_2$ and control

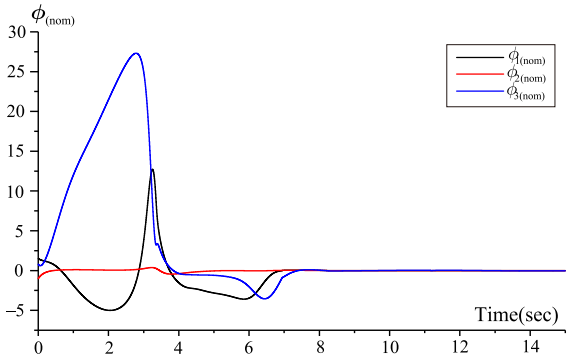

Fig. 7 The trajectory of function $\boldsymbol{\phi}_{(nom)}$

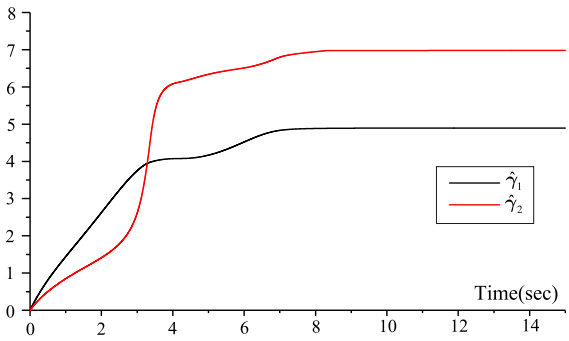

Fig. 8 The trajectories of adaptive gains

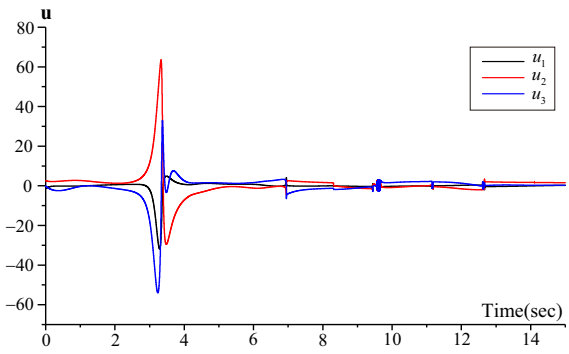

Fig. 9 The trajectory of control input **u**

input **u** are all bounded, as depicted from Figs. 7, 8 and 9, respectively.

8 Conclusion

In this paper, an adaptive SMC scheme is successfully proposed for a class of perturbed FO nonlinear systems with matched and unmatched perturbations to solve regulation problems. The advantages of the proposed control system are as follows. (1) The proposed control scheme can be applied to systems with unmatched perturbations. (2) There is no need to know in advance the upper bounds of perturbations and perturbation estimation errors due to the embedded perturbation estimator and adaptive mechanisms. (3) The resultant control system is able to drive the controlled state trajectories into equilibrium point within a finite time. For future study, solving the tracking problems is worth considering.

Acknowledgements The authors would like to thank the Editor, Associate Editor, and the anonymous reviewers for their many helpful comments and suggestions that have helped to improve the quality of this paper. The author Chih-Chiang Cheng is also grateful to the Ministry of Science and Technology of R.O.C. for financial support for this research (MOST 106-2221-E-110-006).

Compliance with ethical standards

Conflict of interest The authors declare that they have no conflict of interest.

References

1. Gabano, J.D., Poinot, T.: Fractional modelling and identification of thermal systems. Signal Process. **91**(3), 531–541 (2011)
2. Sun, F.; Li, Q.: Dynamic analysis and chaos of the 4D fractional-order power systems. In: Abstract and Applied Analysis, vol. 2014 (2014)
3. Xin, B., Zhang, J.: Finite-time stabilizing a fractional-order chaotic financial system with market confidence. Nonlinear Dyn. **79**(2), 1399–1409 (2015)
4. Jesus, I.S., Tenreiro Machado, J.A.: Application of integer and fractional models in electrochemical systems. Math. Probl. Eng. **2012**, 17 (2012)
5. Petras, I., Magin, R.L.: Simulation of drug uptake in a two compartmental fractional model for a biological system. Commun. Nonlinear Sci. Numer. Simul. **16**(12), 4588–4595 (2011)
6. Kassim, S., Hamiche, H., Djennoune, S., Bettayeb, M.: A novel secure image transmission scheme based on synchronization of fractional-order discrete-time hyperchaotic systems. Nonlinear Dyn. **88**(4), 2473–2489 (2017)
7. Bao, H.B., Cao, J.D.: Projective synchronization of fractional-order memristor-based neural networks. Neural Netw. **63**, 1–9 (2015)
8. Shen, J., Lam, J.: Non-existence of finite-time stable equilibria in fractional-order nonlinear systems. Automatica **50**(2), 547–551 (2014)
9. Bao, H., Park, J.H., Cao, J.: Adaptive synchronization of fractional-order memristor-based neural networks with time delay. Nonlinear Dyn. **82**(3), 1343–1354 (2015)
10. Liu, H., Li, S., Cao, J., Li, G., Alsaedi, A., Alsaadi, F.E.: Adaptive fuzzy prescribed performance controller design

for a class of uncertain fractional-order nonlinear systems with external disturbances. Neurocomputing **219**, 422–430 (2017)
11. Geng, L., Yu, Y., Zhang, S.: Function projective synchronization between integer-order and stochastic fractional-order nonlinear systems. ISA Trans. **64**, 34–46 (2016)
12. Rubagotti, M., Estrada, A., Castanos, F., Ferrara, A., Fridman, L.: Integral sliding mode control for nonlinear systems with matched and unmatched perturbations. IEEE Trans. Autom. Control **56**(11), 2699–2704 (2011)
13. Edwards, C., Spurgeon, S.: Sliding Mode Control: Theory and Applications. Taylor & Francis, London (1998)
14. Defoort, M., Floquet, T., Kokosy, A., Perruquetti, W.: Sliding-mode formation control for cooperative autonomous mobile robots. IEEE Trans. Ind. Electron. **55**(11), 3944–3953 (2008)
15. Park, B.S., Yoo, S.J., Park, J.B., Choi, Y.H.: Adaptive neural sliding mode control of nonholonomic wheeled mobile robots with model uncertainty. IEEE Trans. Control Syst. Technol. **17**(1), 207–214 (2009)
16. Wai, R.J., Shih, L.C.: Design of voltage tracking control for DC–DC boost converter via total sliding-mode technique. IEEE Trans. Ind. Electron. **58**(6), 2502–2511 (2011)
17. Gokasan, M., Bogosyan, S., Goering, D.J.: Sliding mode based powertrain control for efficiency improvement in series hybrid-electric vehicles. IEEE Trans. Power Electron. **21**(3), 779–790 (2006)
18. Tavazoei, M.S., Haeri, M.: Synchronization of chaotic fractional-order systems via active sliding mode controller. Physica A Stat. Mech. Appl. **387**(1), 57–70 (2008)
19. Hosseinnia, S.H., Ghaderi, R., Mahmoudian, M., Momani, S.: Sliding mode synchronization of an uncertain fractional order chaotic system. Physica A Stat. Mech. Appl. **59**(5), 1637–1643 (2010)
20. Aghababa, M.P.: Robust stabilization and synchronization of a class of fractional-order chaotic systems via a novel fractional sliding mode controller. Commun. Nonlinear Sci. Numer. Simul. **17**(6), 2670–2681 (2012)
21. Yin, C., Dadras, S., Zhong, S., Chen, Y.Q.: Control of a novel class of fractional-order chaotic systems via adaptive sliding mode control approach. Appl. Math. Model. **37**(4), 2469–2483 (2013)
22. Aghababa, M.P.: Design of a chatter-free terminal sliding mode controller for nonlinear fractional-order dynamical systems. Int. J. Control **86**(10), 1744–1756 (2013)
23. Ni, J., Liu, L., Liu, C., Hu, X.: Fractional order fixed-time nonsingular terminal sliding mode synchronization and control of fractional order chaotic systems. Nonlinear Dyn. **89**(3), 2065–2083 (2017)
24. Chen, D., Liu, Y., Ma, X., Zhang, R.: Control of a class of fractional-order chaotic systems via sliding mode. Nonlinear Dyn. **67**(1), 893–901 (2012)
25. Aghababa, M.P.: Design of hierarchical terminal sliding mode control scheme for fractional-order systems. IET Sci. Meas. Technol. **9**(1), 122–133 (2014)
26. Chen, Y., Wei, Y., Zhong, H., Wang, Y.: Sliding mode control with a second-order switching law for a class of nonlinear fractional order systems. Nonlinear Dyn. **85**(1), 633–643 (2016)
27. Majidabad, S.S., Shandiz, H.T., Hajizadeh, A.: Decentralized sliding mode control of fractional-order large-scale nonlinear systems. Nonlinear Dyn. **77**(1–2), 119–134 (2014)
28. Karami-Mollaee, A., Tirandaz, H., Barambones, O.: On dynamic sliding mode control of nonlinear fractional-order systems using sliding observer. Nonlinear Dyn. **92**, 1379–1393 (2018)
29. Mujumdar, A., Tamhane, B., Kurode, S.: Observer-based sliding mode control for a class of noncommensurate fractional-order systems. IEEE ASME Trans. Mechatron. **20**(5), 2504–2512 (2015)
30. Aghababa, M.P.: A novel terminal sliding mode controller for a class of non-autonomous fractional-order systems. Nonlinear Dyn. **73**(1–2), 679–688 (2013)
31. Liu, H., Pan, Y., Li, S., Chen, Y.: Adaptive fuzzy backstepping control of fractional-order nonlinear systems. IEEE Trans. Syst. Man Cybern. Syst. **47**(8), 2209–2217 (2017)
32. Wei, J., Zhang, Y., Bao, H.: An exploration on adaptive iterative learning control for a class of commensurate high-order uncertain nonlinear fractional order systems. IEEE CAA J. Autom. Sin. **5**(2), 618–627 (2018)
33. Bataghva, M., Hashemi, M.: Adaptive sliding mode synchronisation for fractional-order non-linear systems in the presence of time-varying actuator faults. IET Control Theory Appl. **12**(3), 377–383 (2018)
34. Zhang, R., Yang, S.: Robust synchronization of two different fractional-order chaotic systems with unknown parameters using adaptive sliding mode approach. Nonlinear Dyn. **71**(1–2), 269–278 (2013)
35. Maheri, M., Arifin, N.M.: Synchronization of two different fractional-order chaotic systems with unknown parameters using a robust adaptive nonlinear controller. Nonlinear Dyn. **85**(2), 825–838 (2016)
36. Shao, S., Chen, M., Yan, X.: Adaptive sliding mode synchronization for a class of fractional-order chaotic systems with disturbance. Nonlinear Dyn. **83**(4), 1855–1866 (2016)
37. Cheng, C.-C., Chiang, Y.-C.: Design of nonsingular adaptive terminal backstepping controllers with perturbation estimation for nonlinear systems in semi-strict feedback form. IET Control Theory Appl. **11**(10), 1589–1595 (2017)
38. Podlubny, I.: Fractional Differential Equations. Elsevier, Amsterdam (1998)
39. Zhao, Y.; Wang, Y.; Liu, Z.: Finite time stability analysis for nonlinear fractional order differential systems. In: 32nd Chinese Control Conference (CCC), China, pp. 487–492 (2013)
40. Cheng, C.C.; Chang, M.W.: Design of derivative estimator using adaptive sliding mode technique. In: American Control Conference, Minneapolis, pp. 14–16 (2006)
41. Tao, G.: Adaptive Control Design and Analysis. Wiley, New York (2003)
42. Qian, D., Li, C., Agarwal, R.P., Wong, P.J.Y.: Stability analysis of fractional differential system with Riemann–Liouville derivative. Math. Comput. Model. **52**(5–6), 862–874 (2010)